

2 Lab 4: Optical Pumping of Rubidium and Magnetic Field Effects (OPT)

3 SHRIHAN AGARWAL¹

4 ¹ University of California, Berkeley, Department of Astronomy, Berkeley, CA 94720

Abstract

In this lab, we investigated the transitions within the atomic structures of Rubidium isotopes ^{85}Rb and ^{87}Rb by driving these transitions using optical pumping. We split the hyperfine energy levels in these isotopes by utilizing a set of Helmholtz coils and appropriate current levels to obtain the Zeeman splitting. We gained an understanding of the quantum mechanics principles that describe the internal laws governing the atom's behaviour by examining Zeeman energy levels. We examined the settings on the different instruments and determined that the appropriate temperature for the Rubidium bulb was between 40 °C and 45 °C. We measured the resonant frequency applied to de-pump the atoms as a function of the magnetic field. With this information, we deduced the ambient field strength at Berkeley, California, to be 0.444 ± 0.002 G for ^{85}Rb and 0.414 ± 0.002 G for ^{87}Rb . We were also able to determine the ratio of the nuclear spin between the isotopes and thus, the spin to be $I_{85} = 2.537 \pm 0.007$ and $I_{87} = 1.545 \pm 0.003$. By modulating the amplitude of the magnetic field lamp, we were able to obtain pumping and relaxation time of the vapor to be 3.2 ms and 41 ms, respectively.

1. INTRODUCTION

In this study, Optically Detected Magnetic Resonance (ODMR) spectroscopy is employed to determine the magnetic moment of Rubidium atoms and the strength of the background magnetic field. To prepare the Rubidium atoms for spectroscopic analysis, optical pumping is used, a technique that polarizes the atoms, discovered by Alfred Kastler in the 1950s. By introducing an external magnetic field, Zeeman splitting further splits the hyperfine states of the atoms, allowing for the detection of transitions between Zeeman states and indirect measurement of the nuclear spins of Rubidium isotopes. Quantum mechanics characterizes the internal structure of atoms, and the set of quantum states in atoms contains information on the motion and internal spin of electrons and nuclei.

Optical pumping is a crucial technique in atomic, molecular, and optical physics, as well as laser physics, facilitating the study of different atoms and molecules. Furthermore, this study analyzes the relationship between the resonance frequency and the external magnetic field to measure the relaxation time and pump of the Rubidium vapor cell and the ambient magnetic field strength in Berkeley, California.

We briefly describe Background Research Theory for Optical Pumping in Section 2. We discuss the experimental design for our particular setup in Section 3. The raw data collected and analysis done is described in Section ???. Lastly, the conclusions are presented in Section 6.

2. BACKGROUND RESEARCH AND THEORY

35 2.1. Atomic Structure of Rubidium

Rubidium, an alkali metal with atomic number 37, is found in nature in two isotopes: Rb-85 and Rb-87, with the former being more abundant. In the electronic ground state, Rubidium has 36 electrons filling states in a closed, inert shell, with the last valence electron occupying the 5s orbital. When excited, the valence electron moves to the 5p orbital, which is about 1.6 eV higher in energy than the 5s orbital. Rubidium has additional complexity due to the angular momentum states of the electron orbital angular momentum L, electron spin S, and nuclear spin I. The

41 ground state has $L = 0$ and the first excited state has $L = 1$. The electron spin is $S = 1/2$, and the nuclear spin is $I = 5/2$ for Rb-85 and $I = 3/2$ for Rb-87. These states interact to produce fine, hyperfine, and Zeeman splittings that cause energy level splitting at smaller scales than the order of eV excited states. These corrections can be described by the fine, hyperfine, and Zeeman splittings of the atomic energy structure.
 42
 43
 44
 45

46 2.2. Fine Structure

Rubidium's fine structure correction arises from the relativistic interaction between the electron's orbital and spin angular momenta and the nuclear spin. The Hamiltonian equation describes this coupling and is represented by $H\nu = LS$. While Hf does not commute with L and S , it does commute with S^2 and L^2 , resulting in a total angular momentum $J=L+S$. The eigenvalues of Hf are proportional to

$$\frac{\hbar^2}{2} [j(j+1) - l(l+1) - s(s+1)]$$

47 , which splits the 5p excited state of Rubidium into $J=1/2$ and $3/2$, leading to the $^2P_{1/2}$ and $^2P_{3/2}$ states.
 48

49 The fine energy correction affects the optical spectrum as transitions from the ground state to the $^2P_{3/2}$ state require
 50 a wavelength of $\lambda=780$ nm, while transitions to the $^2P_{1/2}$ state require a wavelength of $\lambda=795$ nm. This fine structure
 51 splitting is not present in the 5s ground state, where electron angular momentum is 0, and therefore no first-order
 52 correction is needed in the s orbital. The order of the fine splitting is 0.04 eV, which is relatively small but still
 53 significant for precise spectroscopy analysis. This fine structure splitting is an important feature of Rubidium's atomic
 structure and plays a crucial role in optical physics research.

54 2.3. Hyperfine Structure

55 The hyperfine structure splitting in Rubidium is a result of the interaction between the nuclear spin and the electron's
 56 angular momentum, giving rise to a second-order correction to the atomic energy levels. However, this splitting is
 57 much smaller than the fine structure splitting due to the relatively weak interaction between the nuclear magnetic
 58 dipole moment and the electron. In the absence of an external magnetic field, the energy eigenstates of the atom are
 59 the total angular momentum eigenstates, which can be expressed as $F = I + J$, where I is the nuclear spin and J is the
 60 electron angular momentum. This leads to many states with definite total angular momentum quantum number F .
 61 In Rubidium, the hyperfine structure splitting is different for the two isotopes due to their different nuclear spins. For
 62 example, the ground state of Rb-87 has $J = 1/2$ and $I = 3/2$, resulting in energy states separated by $E_{hfs} = h \times 6.8\text{GHz}$
 63 with total angular momentum quantum numbers of $F = 1$ and $F = 2$. For Rb-85, the s and $^2P_{1/2}$ states have $F = 2$,
 64 3 hyperfine levels, while for Rb-87, the s and $^2P_{1/2}$ states have $F = 1, 2$ hyperfine levels.

65 2.4. Zeeman Splitting

66 In the presence of an external magnetic field, the hyperfine structure of an atom is further split into sub-levels, a
 67 phenomenon known as Zeeman splitting. This occurs due to the interaction between the magnetic dipole moment
 68 of the atom's electrons and the magnetic field. The strength of the magnetic field, the angular momentum quantum
 69 number of the electron, and the electron's g-factor, which measures its magnetic moment, determine the magnitude of
 70 the splitting. To determine the magnetic field strength required for resonance between two hyperfine levels in an atomic
 71 system, the Breit-Rabi formula is used. This formula accounts for both the magnetic field and the radio frequency
 72 (RF) radiation effects on the energy levels.

The equation

$$H_{hfs} = -\mu_I(B_J + B_{\text{ext}}) - \mu_J B_{\text{ext}}$$

73 represents the hyperfine structure Hamiltonian, where μ_I and μ_J are the magnetic dipole moments of the nucleus and
 74 g_L is the Lande g-factor. We can use the weak field limit to manipulate the extrinsic term

$$-(\mu_I + \mu_J)B_{\text{ext}},$$

75 as it is the only term we can change in the experiment. By relating the energy difference between two Zeeman states
 to the magnetic field, we obtain the Breit-Rabi formula

$$\frac{\nu}{B_{\text{ext}}} = \frac{2.799 \text{ MHz}}{2I + 1 \text{ G}}, \quad (1)$$

76 where ν is the resonance frequency. This formula is derived using the fact that $g_J = 2$ and $\mu_B = e\hbar/2m_e$.

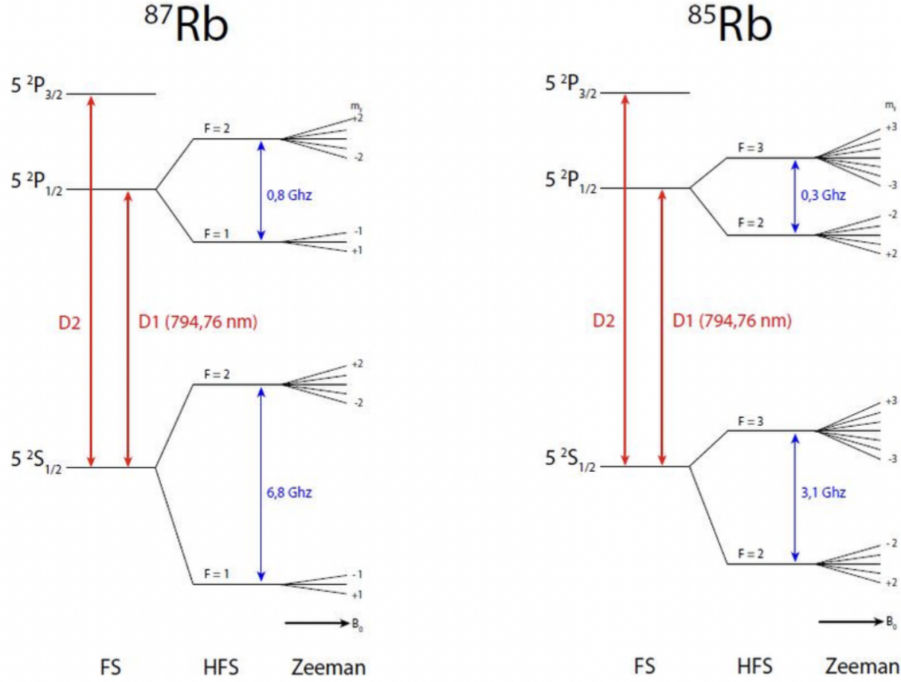


Figure 1: Hyper-fine Structure Splitting of Rb-85 and Rb-87 along with their respective D1 and D2 lines.

2.5. Optical Pumping Principle

In this experiment, the Zeeman energy transitions in the electron ground state of rubidium atoms are studied using optical pumping and radio frequency magnetic fields. Spin polarization is generated through optical pumping, which is essential to measure the transitions. Circularly polarized infrared light drives transitions that increase the magnetic quantum number by 1, resulting in atoms being pumped towards states with larger m_F values. After many cycles of absorption and emission, the population of atoms in the vapor is prepared in the electronic ground state with the highest value of m_F . Radio frequency magnetic fields are then used to induce transitions between hyperfine states, which are measured by observing the change in the distribution of atoms in the hyperfine states.

When photons are absorbed or emitted, they transfer an energy of $h\nu$. To induce transitions between states, we irradiate atoms with radio waves at the exact frequency corresponding to the energy transition between the states. The energy transferred between states is quantized. However, at room temperature, matter does not move fast enough to rise up to levels needed to produce absorption or emission spectra. Therefore, we heat up the rubidium to obtain these transitions.

The principle of optical pumping is illustrated in Figure 2, which shows the energy level transitions that are desired in this experiment. Level A and B are populated by some atoms, and we aim to excite or de-excite them in order to produce the desired transitions. The energy levels increase in energy from A to C, and the quanta of energy required to excite atoms from A to C is different from that required to make a B to C transition.

If we provide the atoms with the exact energy needed for AC transitions, eventually, with time, all the A level atoms will be excited to C. After some time, when they de-excite, they can make transitions down to B or A with equal probability. If they end up in A, they can make the transition to C again, but if they end up at B, they do not have the right energy required to be excited to C. Thus, they are essentially "stuck" in level B. Eventually, all the level A atoms will reach level B after de-exciting. This state of all the atoms ending up in the B state is called completely pumped.

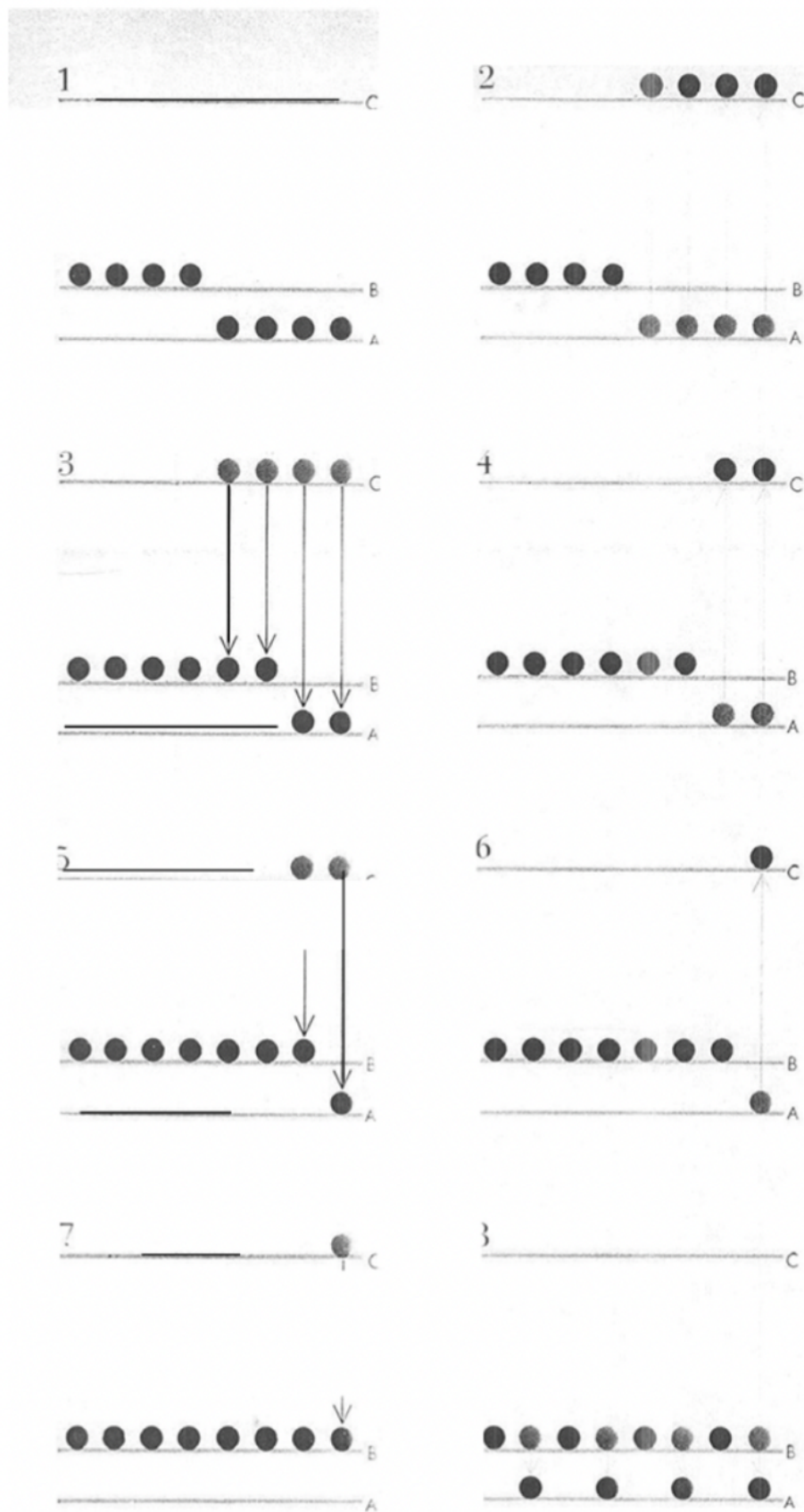
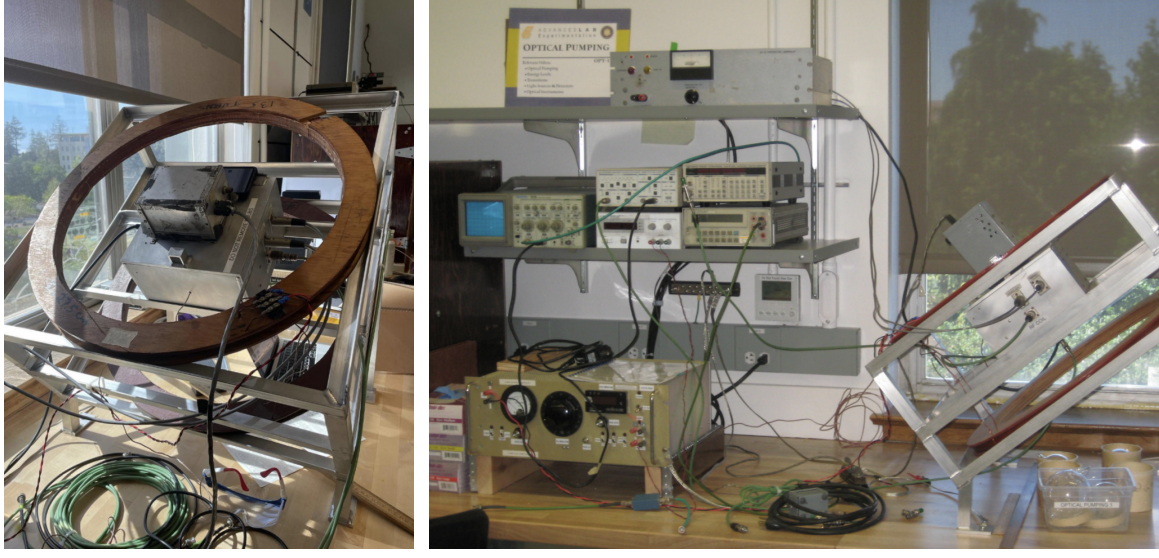


Figure 2: Transition between levels A, B,C. All atoms from state A are pumped to state B.



(a) Close-up of the coils assembly.

(b) Set-up of the whole apparatus.

Figure 3: Transition between levels A, B, C. All atoms from state A are pumped to state B.

104 2.6. *Optically Detected Magnetic Resonance*

105 The principle of optical pumping is based on the creation of a "dark state" where the optically pumped state
 106 does not absorb any light. This dark state enables the detection of radio frequency magnetic transitions in atomic
 107 vapor through optical measurements, which is known as "optically detected magnetic resonance" (ODMR). When
 108 the atomic vapor is in the pumped state, a photodetector measuring the transmitted light will record higher levels of
 109 light. However, applying a resonant radio frequency magnetic field will cause the atoms to exit the optically pumped
 110 state, resulting in absorption of the incident pumping light and lower readings from the photodetector.

111 In the case of Rb-85, the energy level transitions are characterized by the second order splitting of the $^2S_{1/2}$ state
 112 into $F = 2, 3$, and the Zeeman splitting among $-2 \leq m_F \leq 2$ and $-3 \leq m_F \leq 3$. The circularly polarized light can
 113 drive transitions for absorption of $\Delta m_F = +1$ and emission of $\Delta m_F = -1, 0, +1$. The transitions from $^2S_{1/2}$ ground
 114 state to $^2P_{1/2}$ excited state falls under the D1 transitions and split into $F = 2$ and 3 . The hyperfine excited state
 115 with m_F at $-3S$ can only go down to values of $-3S, -2S, -1S$ with equal probability and cannot be absorbed by $m_F =$
 116 $3S$. As a result, the rubidium vapor will be fully saturated in the highest $m_F = 3$ state in the $F=3$ hyperfine ground
 117 state. This principle applies to Rb-87 as well, which will be saturated in its $m_F = 2$ hyperfine ground state. Therefore,
 118 rubidium vapor is pumped and will not absorb light since both isotopes are in their highest hyperfine ground state.
 119

120 However, when all the D2 transitions are driven by the light in the lamp, the pumped state in Rb-85 is no longer
 121 dark. In this state, absorption is now possible since the hyperfine excited states now have a range of F values, including
 122 $1, 2, 3, 4$. Consequently, when $m_F = 3S$, the system transitions up to $m_F = 4P$ and returns to $m_F = 3S$, resulting
 123 in continuous absorption. The same argument applies to the pumped state of Rb-87. By applying an orthogonal
 124 magnetic field via the RF coil, we can de-pump the vapor by supplying the Zeeman energy between neighboring states,
 125 enabling emission to lower states and absorption to excited states. This absorption results in less light passing through
 126 the vapor, leading to a drop in signal intensity received by the photodiode. Precisely measuring this drop allows for
 127 measurements of the resonance frequency of rubidium.
 128

129 3. APPARATUS

130 In this experiment, several pieces of equipment are used to generate and measure signals. A DS345 function generator
 131 is used to generate a signal, which is then sent to a coil driver and an oscilloscope. The coil driver controls
 132 the Helmholtz coils that generate a magnetic field inside the light-proof box containing the vapor cell. The controller
 133 also controls the lamp inside the box that produces the photons required for optical pumping. The temperature of

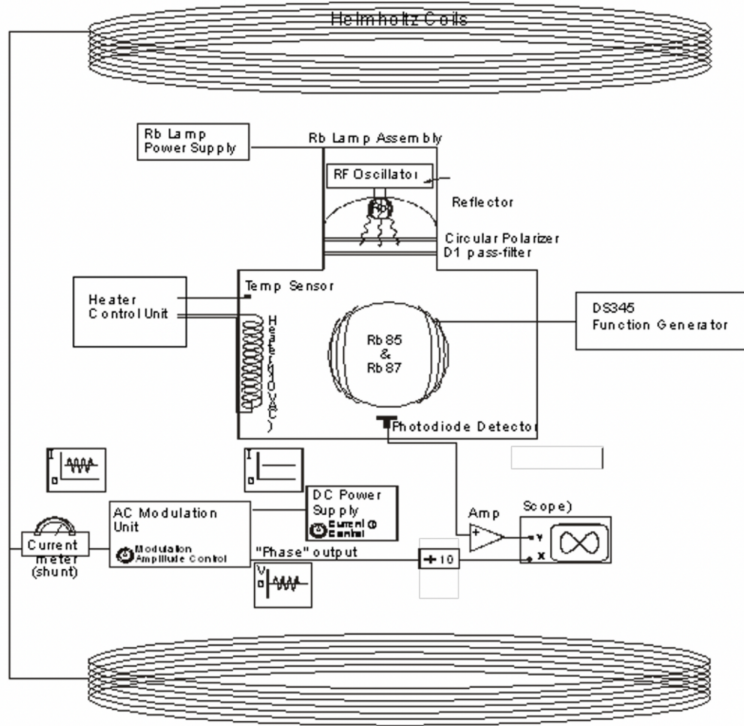


Figure 4: In-depth diagram of apparatus and experimental setup (Source: Lab Manual).

the vapor cell and the light bulb is maintained using a heater connected to the box, with an optimal temperature of 40-45°C for data collection. The intensity of light passing through the Rubidium vapor cell is measured using a photodiode placed on the opposite side of the lamp. The signal from the photodiode is amplified using an SR560 Pre-amp before being fed into the oscilloscope. At the beginning of the experiment, the signals from the function generator and amplifier are used, while the outputs from the coil driver and amplifier are used in the second half of the experiment.

A spherical glass bulb coated with a thin wax layer is used as an atomic vapor cell. The cell is filled with a low density buffer gas and a small amount of rubidium. The amount of rubidium in the cell can be controlled by changing the temperature. The buffer gas in the cell diffuses rubidium for a long period of time before colliding with the glass cell, giving the Rb atoms enough chances to absorb and emit photons. The Heater Control Unit monitors the temperature of the cell, and measurements are made when the heater switch is off to avoid the heating resistors' stray magnetic field's effect on measurements.

Optical pumping optics generate photons from a light source containing Rb gas that has been electronically discharged. The emitted light is circularly polarized by passing through a polarizing filter and an interferometric "D1 pass filter," which only allows light with wavelengths near 795 nm to travel through. The light then passes through the atomic vapor cell, and the outgoing light intensity is measured by a photodiode. The photodiode current is amplified by an SRS SR560 amplifier, and the output signal is sent to an oscilloscope.

The atomic vapor cell is positioned between two electromagnet coils that are connected in series. A SRS DS345 function generator provides a sinusoidal current to these coils, generating a radio frequency magnetic field that runs perpendicular to both the optical axis and the axis of the external magnetic field. This magnetic field is properly oriented to drive Zeeman transitions within the Rubidium vapor.

To prevent interference from room light and ensure accurate detection of the low-intensity optical signal from the Rubidium lamp, the atomic vapor cell, heater, optical pumping optics, and RF coils are enclosed within a light-proof and thermally insulated box. The box also serves to maintain a stable temperature over long periods of time, allowing

161 users to record measurements with the heating unit turned off.
 162

163 The Helmholtz coils generate a nearly constant magnetic field along the z-axis, located outside the light proof box.
 164 An AC and DC current source drives the Helmholtz coils, and the AC voltage, with an additional variable phase
 165 shift, is fed into the oscilloscope that measures the photodiode signal. The DC current controls the Zeeman resonance
 166 frequency of the Rubidium vapor, while the AC current modulation provides an accurate method of measuring the
 167 resonance condition. The axial magnetic field produced by the Helmholtz coil is given by the relation,

$$168 \quad B_z = 0.9 \times 10^{-2} Ni \frac{G}{mA} \quad (2)$$

169 An amplifier amplifies the signal, making it easy to read, and a function generator generates a signal that is sent to
 170 both a coil driver and an oscilloscope. The oscilloscope enables us to visualize the signals.

171 4. PROCEDURE

172 To begin the experiment, we first had to understand how to use the set-up. We carefully examined the experimental
 173 set-up and compared it to the block diagram, taking note of all the connections and identifying each unit's function.
 174 We were particularly cautious when inspecting the inside of the light-proof box, paying close attention to the fragile
 175 glass vapor cell and the optical filters. We then turned on all the equipment, making sure not to exceed the suggested
 176 values as directed by the manual. For instance, we made sure not to run the current in the Helmholtz coil above 3A
 177 and kept the temperature of the light-proof box below 55°C to avoid any issues. We monitored the photodiode signal
 178 and turned on the rubidium lamp, which emitted light that we detected on our photodiode at a current of 25-30mA.
 179 We adjusted the SR560 pre-amplifier at various points during the experiment, starting by selecting Input 'A' with the
 180 DC/GND/Ac button on the AC position. We set the gain to 500, the LF Roll-off to 0.1Hz, and the HF Roll-off to
 181 10kHz, with both filters set at 6dB per octave, making adjustments later to discover why these settings were a good
 182 starting point. We encountered an issue with the SR560 sometimes going into "overload," but we were able to reset
 183 the unit by pressing the OL REC button.
 184

185 4.1. Optically Detected Magnetic Resonance

186 To observe the Zeeman resonances in Rubidium, the experiment begins by sweeping an RF signal over a large
 187 frequency range until a pattern is observed. Optically pumping the Rubidium population to the highest m_F state
 188 creates a "dark state" in which the atoms can no longer absorb photons, resulting in the highest photodiode signal.
 189 We then sweep the RF signal through the frequencies that correspond to the specific frequency shift, causing spikes in
 190 the photodiode signal as the Rubidium population transitions from "dark" to non-dark states. This process yields two
 191 different peaks, one for each isotope in the vapor cell, allowing for the measurement of Zeeman resonances. To observe
 192 these resonances, we apply a DC magnetic field to the Rubidium vapor cell and sweep a wide range of RF frequencies
 193 using the DS 345 generator while monitoring the photodiode signal. This method is not precise or accurate in finding
 194 the Zeeman resonances. The procedure involves heating the light-proof box to dissolve enough Rubidium atoms in
 195 the vapor cell, running a DC current of 1A to the Helmholtz coil and measuring the current accurately by reading the
 196 DC voltage across the shunt resistor. The magnetic field also sums up other external fields. The DS 345 unit is set
 197 to a sinusoidal current and linearly swept frequency, and we measure the photodiode signal amplifier versus the RF
 198 magnetic field frequency. We obtain the ODMR signal by adjusting the positioning and divisions of each axis.
 199

200 4.2. Bulb Temperature

201 To optimize the Optically Detected Magnetic Resonance (ODMR) experiment, we tested the effect of temperature
 202 on the ODMR signal. We gradually increased the temperature of the light-proof box to the maximum temperature
 203 we could reach, which was 45 degrees Celsius, and recorded the ODMR signal for each isotope on the oscilloscope.
 204 We then turned off the heaters and recorded how the ODMR signal height changed over time as the temperature
 205 decreased. We graphed the measurements of the ODMR signal height for each isotope against the box temperature
 206 from 25 to 45 degrees Celsius, and determined that 45 degrees Celsius provided the optimal results.

207 4.3. *Lock-In Detection of Resonance*

To detect the resonance signal, we used the lock-in detection method, which involves applying a modulation to the experimental apparatus at a high frequency and then measuring the variation of a measured signal at the modulation frequency. This method is slow, but has two advantages over the slow DC approach. First, it detects an AC signal rather than a DC signal. Second, it allows us to take derivatives of the photodiode signal versus current. We started by turning on the field modulation by flipping the "Field" switch on the Coil Driver panel and also turning on the "PhaseOut" output by flipping the "PhaseSwitch." We recorded this on the X-axis (Channel 1) of our oscilloscope, while still recording the amplified photodiode voltage on the Y-axis (Channel 2). In order to take measurements for the negative orientation of the Helmholtz field, we reversed the polarity of the coils and hence flipped the direction of the supplied current.

To find the Zeeman resonance for each isotope, we set the rf function generator to the estimated resonance frequency (with no frequency modulation), and then tuned the DC current around 1.0A until the resonance was observed. At resonance, we saw a Lissajous curve on the oscilloscope. We took measurements for resonance frequencies at various currents, the resonance frequency at 0 DC current, and the zero-field resonance.

223 4.4. *Optical Pumping Timescale*

To observe coherent Rabi oscillations, we can utilize a low-frequency amplitude-modulated sinusoidal signal from the RF generator and trigger the scope in synchronization. However, various factors such as collisions, inhomogeneous magnetic fields, light scattering, and the glass cell wall can dampen the Rabi oscillation. Additionally, this setup can help us in observing the pump and relaxation times of the Rubidium population. We achieve this by turning the RF field on and off at a particular resonance frequency under a magnetic field while utilizing a square wave to modulate the collected data. By analyzing the photodiode response as the field is switched on and off, we can extract valuable information about the pump and relaxation times of the atoms.

231 5. ANALYSIS

This analysis has the following three objectives:

- Determine the nuclear spin values of the two rubidium isotopes, Rb-85 and Rb-87.
- Verify the Breit-Rabi formula by varying magnetic field and resonance frequency.
- Determine the ambient (primarily Earth's) magnetic field.

236 5.1. *Analysis 0: Response-Temperature Relation*

For our first test of the equipment, we wanted to understand how the detector response varies with changing temperature of the vapor cell. We believe there is strong systematic error in our temperature measurements, causing our curve to be shifted compared to the expected curve in the lab manual. However, quantifying this error is not necessary for our optical pumping goals. We present a plot of our results in Figure 5.

241 5.2. *Analysis 1: Frequency-Current Relation*

The resonance frequency changes with the changing magnetic field as specified by the Breit-Rabi formula (Eq. 1). We vary the magnetic field using the current passed through the Helmholtz coils, and can calculate the effective magnetic field due to this current using Eq. 2.

Since the data has been taken at both positive and negative current polarity (+B_z and -B_z) for both Rb-85 and Rb-87, we have 4 different sets of data. We fit each of the datasets individually before combining them.

A linear fit was chosen, as the fit was within uncertainty expectations, and agreed with the Breit-Rabi formula and Eq. 2, which together claim that $I \propto B \propto \nu$. The fit was performed minimizing least-squared loss, and took into account uncertainties, with equal weights (the uncertainties on all data points were the same). We further checked the chi-squared value of the fit to judge the quality of the fit. Other fits attempted did not achieve the residuals that

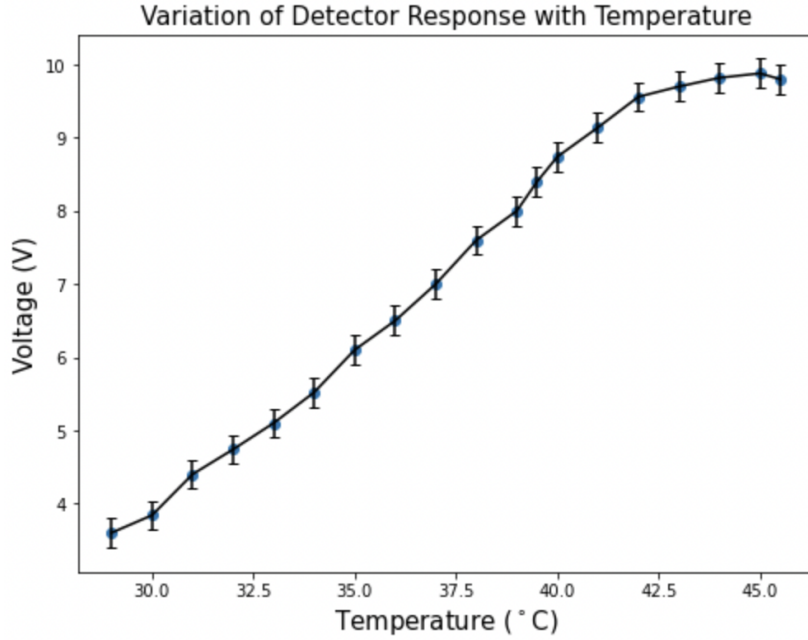


Figure 5: Temperature response of the detector between a range of values.

253 a linear fit could, without adding an increase in degrees of freedom. A chi-squared fit was done only y-uncertainty (as
 254 specified in the lab report), even though uncertainties in both current and frequency were present. This caused the
 255 chi-squared fitting to appear to underestimate the errors.

256
 257 The slope of the fits determine the frequency-current response (the constant in the proportionality), while the
 258 y-intercept marks the zero-current (ambient field) resonance frequency, and the x-intercept marks the zero-frequency
 259 (zero-field) current.

260 **Rb-85, Positive Polarity:**

- 261 • Slope: 2.025 ± 0.004 MHz/A
- 262 • Predicted Ambient Field Resonance: 196.07 ± 3.5 kHz
- 263 • Predicted Zero Field Current: -0.097 ± 0.002 A
- 264 • Chi-squared: 2.229

266 **Rb-85, Negative Polarity:**

- 267 • Slope: 2.046 ± 0.009 MHz/A
- 268 • Predicted Ambient Field Resonance: 218.34 ± 8.31 kHz
- 269 • Predicted Zero Field Current: -0.107 ± 0.004 A
- 270 • Chi-squared: 3.433

271 **Rb-87, Positive Polarity:**

- 272 • Slope: 3.011 ± 0.009 MHz/A
- 273 • Predicted Ambient Field Resonance: 277.5 ± 8.25 kHz
- 274 • Predicted Zero Field Current: -0.092 ± 0.002 A

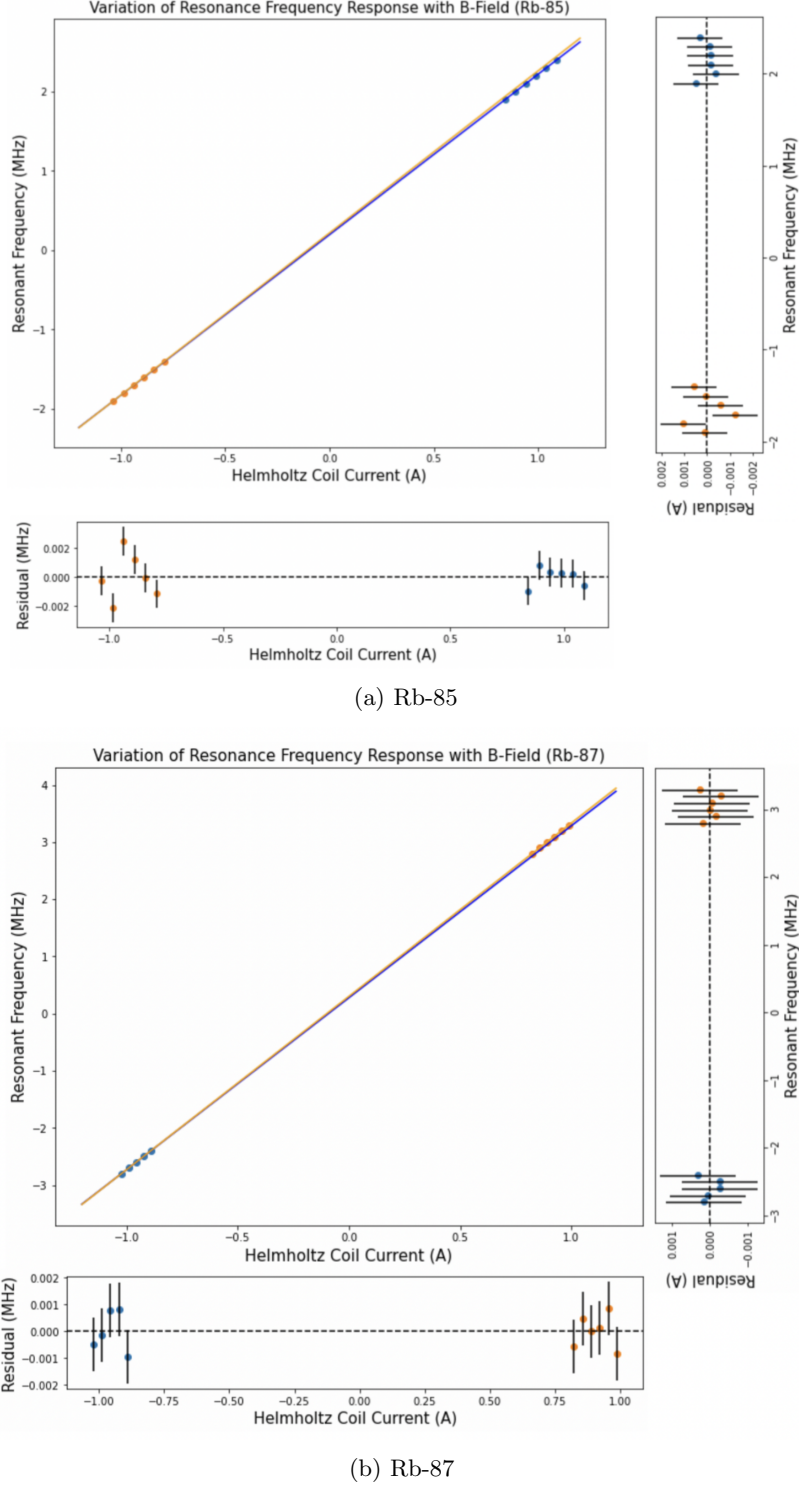


Figure 6: Variation of resonance frequency with Helmholtz coil current. Residuals in current are shown on the right, and residuals in frequency are shown on the bottom, with respective error-bars for all 4 fits. The top set is for Rb-85, and the bottom set is for Rb-87. Though frequency cannot be negative, we flip sign for the negative polarity current for consistency in the fit.

- 275 • Chi-squared: 1.992

276 **Rb-87, Negative Polarity:**

- 277 • Slope: 3.036 ± 0.005 MHz/A
- 278 • Predicted Ambient Field Resonance: 302.04 ± 4.64 kHz
- 279 • Predicted Zero Field Current: -0.099 ± 0.002 A
- 280 • Chi-squared: 2.457

281 These values correspond to the slope, y-intercept, and x-intercept of the fit respectively, for each of the 4 fits. Once
282 again, the chi-squared indicates an underestimation of errors as the x_i uncertainties are unaccounted for.

283 *5.3. Analysis 2: Determining Nuclear Spins*

284 *5.3.1. Method 1*

285 From the fits, we know the slopes, which correspond to the constant of proportionality between the current and
286 frequency response. Ignoring the ambient magnetic field contribution since only the ratio between the frequencies
287 matters, we find,

$$288 \frac{\nu_{87}}{\nu_{85}} = \frac{2I_{85} + 1}{2I_{87} + 1} = \frac{m_{87}}{m_{85}} \quad (3)$$

289 where m_{87} and m_{85} are the slopes of the two frequency-current responses. We combine the positive and negative
290 polarities, re-fit for m_{87} and m_{85} , and calculate the ratio to find,

$$291 \frac{\nu_{87}}{\nu_{85}} = 1.485 \pm 0.006 \quad (4)$$

292 Plugging in half-integral values for I_{87} and I_{85} , we find that the best fit ratio is $I_{87} = 3/2$ and $I_{85} = 5/2$.

293 *5.3.2. Method 2*

294 Using the Breit-Rabi formula directly, we find that,

$$295 I = \frac{2.799 \text{ MHz} \cdot B_{\text{ext}}}{2\nu} - \frac{1}{2} \quad (5)$$

296 Applying this formula for the B/v slope found separately for Rb-85 and Rb-87, we find,

$$I_{85} = 2.537 \pm 0.007$$

$$I_{87} = 1.545 \pm 0.003$$

297 Though the uncertainty is underestimated, we can see that the closest half integral values are indeed 5/2 and 3/2
298 respectively. The uncertainty underestimation and possible systematic errors are likely caused due to multiple reasons.

300 First, the magnetic field calculated theoretically is not necessarily the exact magnetic field the Rubidium atoms
301 experience. This is because there may be a variation in the magnetic field with distance between the coils and
302 variation in the centering of the Rubidium, because the Helmholtz coils may overheat causing non-ideal magnetic field
303 generation, uncertainties due to changes in the ambient magnetic field from neighboring equipment, and temperature
304 fluctuations in the heater causing improper vaporization. Though these effects were mitigated in our experiment
305 setup, the degree of their effect was not accounted for in our analysis.

306 Secondly, the approximations used in the Breit-Rabi formula to reach Eq. 1, used in order to simplify the calculations,
307 may add additional systematic uncertainty. We used the low-field limit of the Breit-Rabi formula, which may affect
308 the accuracy of our half integral estimates.

Polarity	Coil Current (Eq. 2)	Breit-Rabi (Eq. 5)
Positive (0.8903 A)	3.934 +- 0.004 G	4.287 +- 0.002 G
Negative (-0.8397 A)	3.710 +- 0.004 G	3.215 +- 0.002 G

Figure 7: Magnetic field uncertainty comparisons from the coil current calculation and the Breit-Rabi calculation. The difference points to the existence of systematic errors.

310 5.4. Magnetic Field Uncertainty

311 Given possible systematic uncertainties in the magnetic field theoretically estimated by Eq. 2, and the magnetic
 312 field estimated from the resonance frequencies, we perform a calculation to determine them separately. Namely,

$$B_z = 0.9 \times 10^{-2} Ni \frac{G}{mA}$$

313 and

$$314 B_z = \frac{(2I + 1)\nu}{2.799\text{MHz}} G \quad (6)$$

315 In the Table ?? are the results of these calculations alongside their uncertainties, assuming exact half integral values.
 316

317 This process affirms the existence of large systematic errors in the estimation of the current coil's magnetic field
 318 generation, at the location of the vapor cell. As mentioned before, this could be due to variation in the magnetic field
 319 with distance between the coils and the centering of the vapor cell, because the Helmholtz coils may overheat causing
 320 non-ideal magnetic field generation, and the existence of uncertainties due to changes in the ambient magnetic field
 321 from neighboring equipment. The Breit-Rabi formula has also been approximated, and uncertainties in the knowledge
 322 of the Bohr magneton value, and the neglection of nuclear Zeeman energy may cause an incorrect estimation of
 323 magnetic field on the right hand side as well.

325 5.5. Analysis 3: Ambient Magnetic Field

326 A predicted ambient magnetic field can be determined from the fits, and was presented as the y-intercept of the fit
 327 earlier. The values of the predicted ambient field arise from a current of:

328 329 Rb-85 (+ and - polarities):

- 330 • Predicted Ambient Field Resonance: 196.07 ± 3.5 kHz
- 331 • Predicted Zero Field Current: -0.097 ± 0.002 A
- 332 • Predicted Ambient Field Resonance: 218.34 ± 8.31 kHz
- 333 • Predicted Zero Field Current: -0.107 ± 0.004 A

334 335 Rb-87 (+ and - polarities):

- 336 • Predicted Ambient Field Resonance: 277.5 ± 8.25 kHz
- 337 • Predicted Zero Field Current: -0.092 ± 0.002 A
- 338 • Predicted Ambient Field Resonance: 302.04 ± 4.64 kHz
- 339 • Predicted Zero Field Current: -0.099 ± 0.002 A

This means we should expect a zero-field current resonance at a -0.1A input, and two RF resonances at an ambient magnetic field, at about 196-218 kHz and another at 277-305 kHz. This corresponds to the case of exact cancellation of the ambient field, or presence of only an ambient field, respectively.

In experimentation, we find the following values:

Measured Ambient Field Resonances:

$$Rb - 85 : 210.4 \pm 0.1 \text{kHz} (A)$$

$$Rb - 87 : 314.0 \pm 0.1 \text{kHz} (B)$$

Measured Cancellation Zero-Field Current:

$$Both : -0.0983 \pm 0.0010 A (C)$$

Which are near our predicted values from the fit.

Using these measured values, we measure the ambient magnetic field as:

$$A : 0.451 \pm 0.002 G$$

$$B : 0.449 \pm 0.002 G$$

$$C : 0.434 \pm 0.004 G$$

Using the fit, we measure the ambient magnetic field as:

$$Rb - 85 : 0.444 \pm 0.002 G$$

$$Rb - 87 : 0.414 \pm 0.002 G$$

Using an online calculator ?, we can find the estimated Earth magnetic field:

$$\text{Earth's Field at Berkeley, CA} : 0.477 \pm 0.001 G$$

These values, while not in agreement, are similar to the expectations from other studies. We see resonances at these values because at zero field, the resonance should happen at zero frequency according to the Breit-Rabi formula. This means we see a resonance when the ambient field is exactly cancelled.

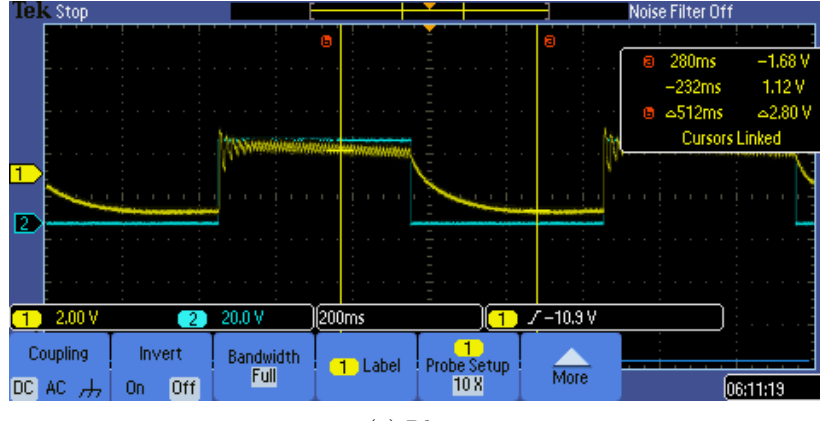
5.6. Analysis 4: Pumping Time

We observe the amount of pumping and relaxation by performing a square wave modulation. This caused the setup to pump and relax repeatedly. Roughly approximating the half life of the decay, we find that the pumping time of the vapor is 3.2ms up and 41ms down.

Rabi-oscillations can be seen throughout the pumping, especially during the pump up. This is because of the cyclical spin oscillations of the atoms when suddenly subjected to an RF field. The pumping time is dependent on the density of Rubidium and the power of the Rubidium lamp.

6. CONCLUSION AND FURTHER WORK

In this lab, we successfully verified the low-field approximation to the Breit-Rabi formula, performed optical pumping of the Rubidium atoms, estimated the nuclear spin of the Rubidium isotopes, calculated uncertainties and systematics in our experimental setup, calculated the ambient magnetic field, and roughly determined the optical pumping timescale. This allowed us to understand the structure of the Rubidium atom in detail, including hyperfine splitting, as well as the effects of an external magnetic field on the Hamiltonian of the atom.



(a) Rb-85

Figure 8: Pumping time decay curve. The pump up is on the order of 1ms, while the decay down is on the order of tens of ms. Rabi-oscillations are visible in the oscilloscope.

We determined the nuclear spins of Rb-85 to be 5/2 and Rb-87 to be 3/2 using two different methods. We determined the ambient magnetic field from the optical pumping setup to be 0.450 ± 0.002 G (A and B) from the ambient field resonances assuming a correct setup for the measurement of resonance frequency and to be 0.434 ± 0.004 G from the ambient field cancellation assuming Eq. 1 holds. We roughly determined the pump up time to be 3.2 ms, and the pump down time to be 41 ms.

We acknowledge that all the measurements were not ideal, and found a general underestimation of uncertainties. Analyzing this in detail we found the magnetic field generation was systematically higher than expected from the Breit-Rabi formula, pointing to issues in the estimation of the number of coils and coil area, a systematic underestimation of the current input into the coil, heating of the coils causing increasing resistance, the centering of the vapor cell, and variation of the magnetic field between the coils. It is also possible the low-field approximation of the Breit-Rabi formula caused an underestimation of the true magnetic field, or both.

For further improvements to this experiment, it may be necessary to directly test, and measure the magnetic field within the coil beside the vapor cell, use the entire Breit-Rabi formula, or ensure the coils remain cool. Additionally, the vapor cell can be checked for centering, and the RF generation can be double checked for systematic uncertainties. Overall, this would improve the accuracy of the experiment.